National Radio Astronomy Observatory
Green Bank, West Virginia
ELECTRONICS DIVISION INTERNAL REPORT NO. 313

Signal Analysis and Blanking Experiments on DME Interference

J. R. Fisher

April 12, 2004

1 Introduction

The frequency range 962 to 1213 MHz is allocated to aircraft radio navigation, mainly used by civilian Distance Measuring Equipment (DME) and a compatible military Tactical Air Navigation (TACAN) system. The air-to-ground transmissions are confined to the 1025 to 1150 MHz range, and the 962-1024 and 1151-1213 Mhz bands are for the ground to air portion of the service. Sharing this band is the radar transponder system which uses 1030 MHz for ground-to-air interrogation and 1090 MHz for air-to-ground responses. Since many aircraft transmitting in the 1025-1150 MHz band are line-of-sight to Green Bank, this frequency range is quite full of strong signals during most of the day. This report is an account of various experiments aimed at understanding the details of signals in this piece of spectrum and attempts to remove them from radio astronomy data.

The DME system uses a time delay method for measuring the distance from an aircraft to a ground station. The aircraft begins determining its distance by transmitting short pulse pairs at a maximum rate 150 pulse pairs per second on the receive frequency of the selected ground station. After a fixed 50 microsecond delay from the received pulse time the ground station transmits a pulse pair back to the aircraft on a frequency either 63 MHz higher or lower than the aircraft transmission frequency. By measuring the delay between transmitted and received pulses, less 50 microseconds, the aircraft's DME unit can determine it's distance from the ground station. This gives the slant-range distance rather than horizontal distance, but the latter can be computed from knowledge of the aircraft's altitude and the elevation of the ground station. Once the aircraft has established a steady dialog with the ground station it slows its pulse rate to a maximum of 24 and 30 pairs per second. Since up to 100 aircraft can simultaneously use the same ground station on the same frequency, the aircraft transmitters jitter their pulse transmission intervals to avoid locking onto ground station pulses intended for other aircraft. See Kline [2] and Forssell [1] for more details.

TACAN uses the same pulse timing structure as DME, but it adds azimuth information to the ground-transmitted pulse intensities. The civilian DME ground stations are generally co-located with VHF Omni-Range (VOR) stations, which provide the azimuth information. VOR operates in the 108 to 118 MHz band.

2 DME Signal Characteristics

DME transmission frequencies are 1 MHz apart. There are 126 aircraft transmission channels running from channel 1 at 1025 MHz through channel 126 at 1150 MHz. There are two transmission modes for each channel. In mode X the ground station transmission frequency is 63 MHz below the aircraft transmission frequency for channels 1-63 and 63 MHz above the aircraft frequency for channels 64-126. In mode Y the ground frequency is 63 MHz above the aircraft frequency for channels 1-63 and 63 MHz below the aircraft frequency for channels 64-126. Hence, in mode Y the ground station transmissions are in the air-to-ground band. To avoid confusion between aircraft and ground station transmissions on the same frequency and to discriminate pulses from random interference, pulses are always transmitted in pairs. From the aircraft in mode X the pulses are 12 microseconds apart, and in mode Y they are 36 microseconds apart. From the ground transmitter the pulses are 12 and 30 microseconds apart in modes X and Y, respectively. Mode X is used much more frequently than mode Y.

The transmitted pulses are approximately gaussian in shape as a function of time with a half-amplitude(voltage)-full-width of 3.5 microseconds.

$$V(t) \propto e^{-0.5(t/\sigma)^2} = e^{-2.7726(t/W)^2} \tag{1}$$

where t is time, and W is the full-width-half-maximum pulse width in the same units as t. Hence, from van Vliet *et al* [3] the individual pulse frequency spectrum will then be gaussian in shape

$$V(f) \propto e^{-0.5(\omega\sigma)^2} = e^{-3.5597(fW)^2} \tag{2}$$

where f is frequency in units of inverse W. The voltage spectrum full-width-half-maximum is then $0.8825/W$, or 0.252 MHz. The power spectrum full-width-half-maximum is $1/\sqrt{2}$ times that, or 0.178 MHz.

The peak pulse power from a transmitter on a large jet aircraft is 300 watts. Manufactures of aircraft transceiver claim useful a range of about 550 km (300 nautical miles) [7], but aircraft altitude and the separations between ground stations on the same frequency will often limit the range to less than 300 km. Smaller aircraft use peak powers on the order of 50 watts, which limits their ideal range to about 250 km. Smaller aircraft fly at lower altitudes and have a shorter line-of sight distance to the ground station. An aircraft at 1700 meters (5000 feet) altitude can expect a range of less that 100 km. The "standard service volumes" [8] have radii of 130 nautical miles (240 km), 40 nm (74 km), and 25 nm (46 km) for high altitude (18,000 to 45,000 feet above ground level), low altitude (1,000 to 18,000 ft AGL) and terminal (1,000 to 12,000 ft) category DME stations, respectively. Some DME facilities are paired with airport localizer transmitters. Localizers are similar to VORs but are designed to work in a limited azimuth sector centered on the approach path to an airport runway. Ground transmitter peak power is between 100 and 1000 watts, depending on the station's intended service.

In the measurements described below I found that the peak power threshold for detecting a single pulse, with a moderate number of false detections, is about ten times the average noise power in a 0.25 MHz receiver bandpass centered on the pulse carrier frequency. This threshold corresponds to a power of 6.9×10^{-16} watts, or -151.6 dBW at the GBT receiver input with a noise temperature of 20 Kelvins. If we assume a transmitter power of 300 watts, a transmitting antenna gain of 0 dBi, and a GBT sidelobe gain of -15 dBi, the maximum free-space distance at which a single pulse can be detected is about 2500 km. The detectable range of a 50-watt pulse is about 1000 km. Neglecting atmospheric refraction, the zero-degree horizon line-of-sight distance to an aircraft at 35,000 feet altitude is about 360 km so any aircraft DME transmitter whose line of sight to the GBT is above the horizon will generally be detectable in the GBT output with a signal filter matched to the pulse bandwidth. An aircraft with a 300-watt transmitter at 500 km distance would be detectable below the horizon if its diffraction loss is less than 14 dB.

As a comparison, the quoted receiver sensitivity of the AMS Model 1118/1119 DME ground station system is -117 dBW for 70% replies, and its minimum antenna gain is +8 dBi [5]. If we again assume a 0 dBi transmitting antenna and 300 watts transmitted power, this corresponds to a useful line-of-sight range of 660 km. This is very close to the claimed useful range of a 300 watt aircraft transceiver.

3 Measured Pulse Properties

Figure 1 shows the composite spectrum seen by the GBT in the frequency range of 1085-1222 MHz at the low end of the tuning range of the 1.15-1.72 GHz,L-band receiver. This spectrum was measured on February 20, 2004 between 12:00 and 14:00 EST. It covers DME channels 65 through 126 and the frequencies of their corresponding mode X ground transmitters above 1150 MHz. The air-to-ground portion of this spectrum is shown expanded in Figure 2. DME signals can be seen in every channel except below 1096 MHz where the radar transponder reply signals at 1090 MHz dominate the spectrum. A careful search for pulses from ground stations above 1150 MHz showed no detectable DME signals in these data.

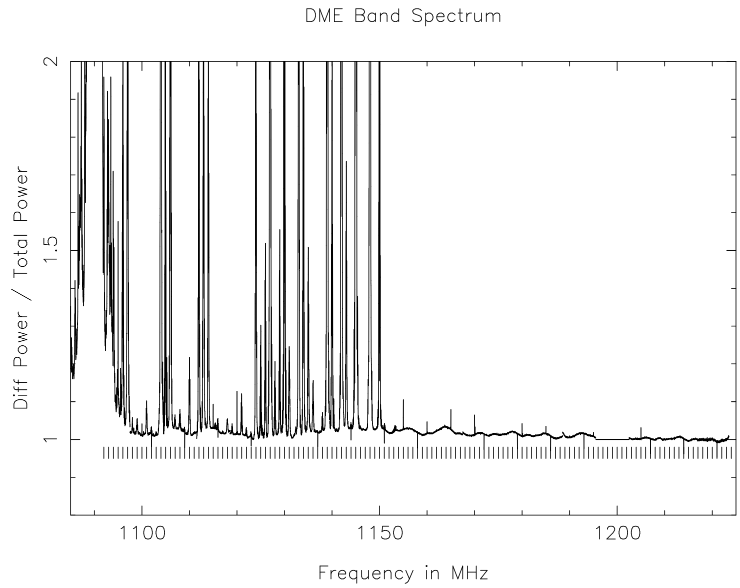

Figure 1: Composite spectrum measured on the GBT of the top half of the aircraft navigation band (DME Channels 65 to 126). Each 7-Mhz spectrum segment is a 5-minute integration normalized to the receiver noise power. The segment near 1200 MHz was used as a reference spectrum so it is shown as a flat line. Hash marks below the spectrum show the DME 1-MHz channel frequencies.

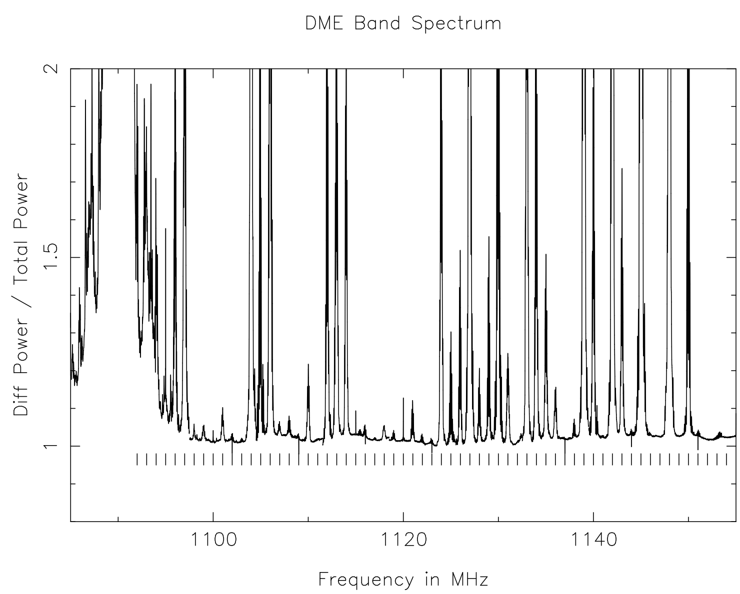

Figure 2: Expansion of the air-to-ground half of the composite spectrum in Figure 1. Hash marks below the spectrum show the DME 1-MHz channel frequencies.

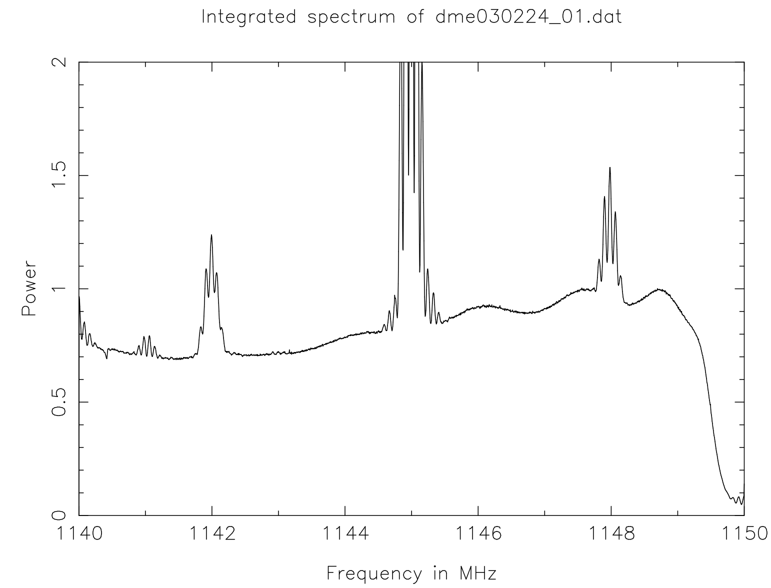

Figure 3: Total power spectrum of the frequency range 1140 to 1150 MHz (DME Channels 116 to 126) using a log periodic antenna directed toward the zenith, 30 seconds of integration, and 5 kHz resolution.

Figure 3 shows the total power spectrum of the 1140 to 1150 MHz passband measured with a log periodic antenna pointed at the zenith near the ground at Green Bank. DME signals can be seen in at least 7 of the 11 channels included in this frequency range.

Figure 4 shows a pair of strong pulses measured at 1142 MHz. These pulses nearly saturated the RF amplifiers so the negative peaks are slightly compressed. Plotted over the pulses are two gaussians with 3.5 microsecond full-width-half amplitude spaced 12 microseconds apart. This particular transmitter appears to truncate its pulses somewhat faster than a gaussian curve, hence the spectral bandwidth will be somewhat wider that the values stated in Section 2. Also, the pulses are a couple of tenths of a microsecond closer together than 12 microseconds. This may be typical of the tolerances to be expected.

Figure 5 shows the Fourier transformed amplitude (voltage) spectrum of the pulses shown in Figure 4. As expected from the measured pulse shape, the amplitude spectrum is wider than would be expected from a gaussian pulse shape of 3.5 microseconds half-amplitude width. Also, the carrier frequency is about 21 kHz lower than the nominal 1142.0 MHz of this transmitter channel. (A manufacturer's DME transceiver brochure [6] states a frequency stability specification of ± 100 kHz.) The 83 kHz modulation period in this spectrum is due to coherent beating of the two pulses.

Figure 6 shows the phase of the pulse carrier across the time of the pulse pair in Figure 4. As expected from the carrier frequency offset found in the pulse spectrum, the phase drifts by about 2.2 radians in the 16 microsecond time span of the two pulses. Also note that the phase within one pulse has a slightly parabolic shape, presumably from a small phase shift in the amplitude shaping circuitry. Otherwise, the carrier phase appears to be contiguous across the two pulses.

Figure 7 shows a fairly typical train of pulses from several aircraft at 1144 MHz. There appear to be at least five transmitting aircraft in this plot as surmised from the tracks of pulse intensity as a function of time. Three of the transmissions began in the time interval shown at about 52.5, 53.0, and 57.5 seconds. Each began with a repetition rate of about 20 pulses per second and then slowed to about 4 or 5 pps. This is a considerably slower pulse rate than the 120-150 and 24-30 pps acquisition and post-acquisition rates described in the DME system descriptions in the literature [1] [2]. A Rockwell-Collins Model DME-42/442 product brochure [6] states that it is capable of scanning three DME channels at 12.5 milliseconds per channel "...so the DME samples each channel 27 times each second. Even when covering three channels at once, it can lock-on in less than one second." This fits the observed behavior of the three pulse tracks in Figure 7. After acquisition the transceiver appears to scan the channels at a slower rate, possibly to conserve power.

The detection threshold used in generating Figure 7 is about ten times the average receiver noise power

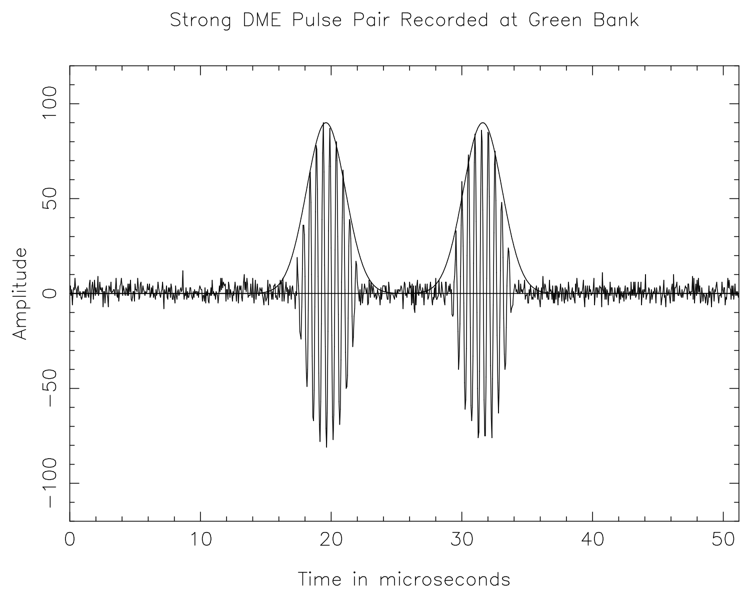

Figure 4: Strong pulse pair measured at 1142 MHz. The waveform is slightly saturated on negative peaks. The gaussian curves are 3.5 microseconds half-amplitude width and 12 microseconds apart.

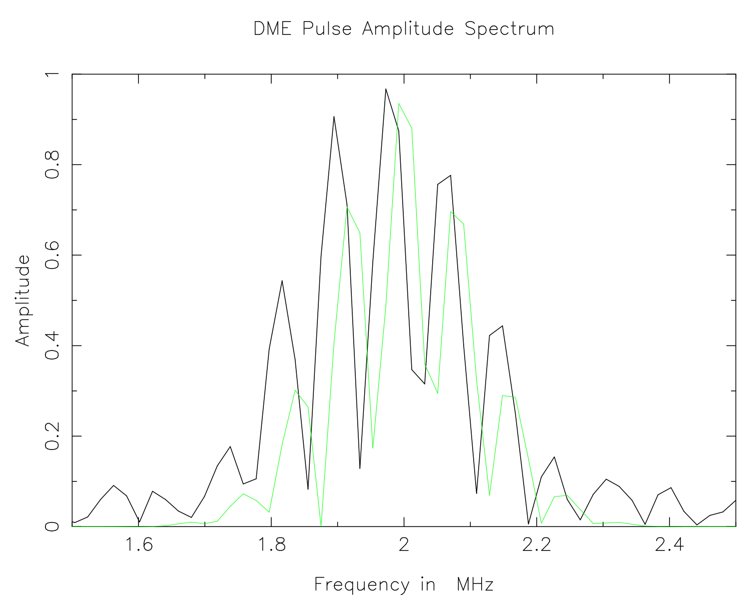

Figure 5: Amplitude spectrum of the pulse pair in Figure 4. The green (lighter) curve is the spectrum expected from a pair of gaussian pulses of 3.5 microseconds amplitude width and 12 microseconds apart with a carrier frequency of 1142.000 MHz.

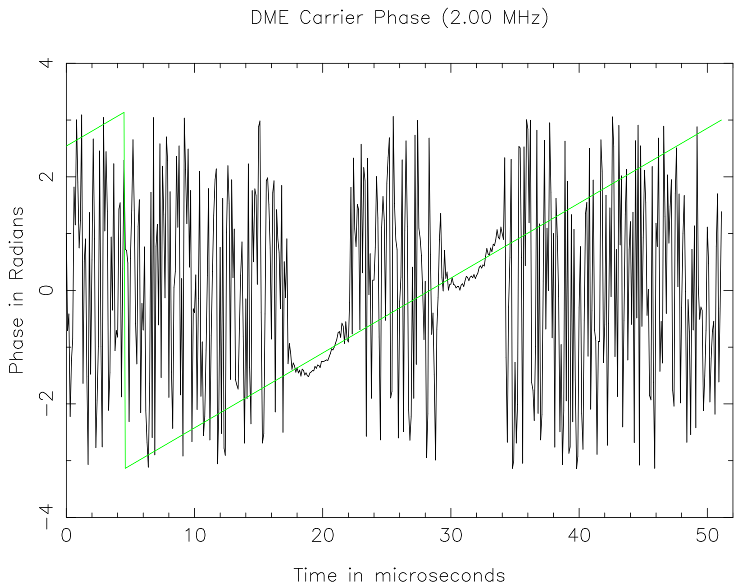

Figure 6: Carrier phase as a function of time across the two pulses shown in Figure 4 assuming a carrier frequency of 1142.000 MHz. The green (lighter) curve shows the phase drift expected from a carrier 21 kHz lower in frequency.

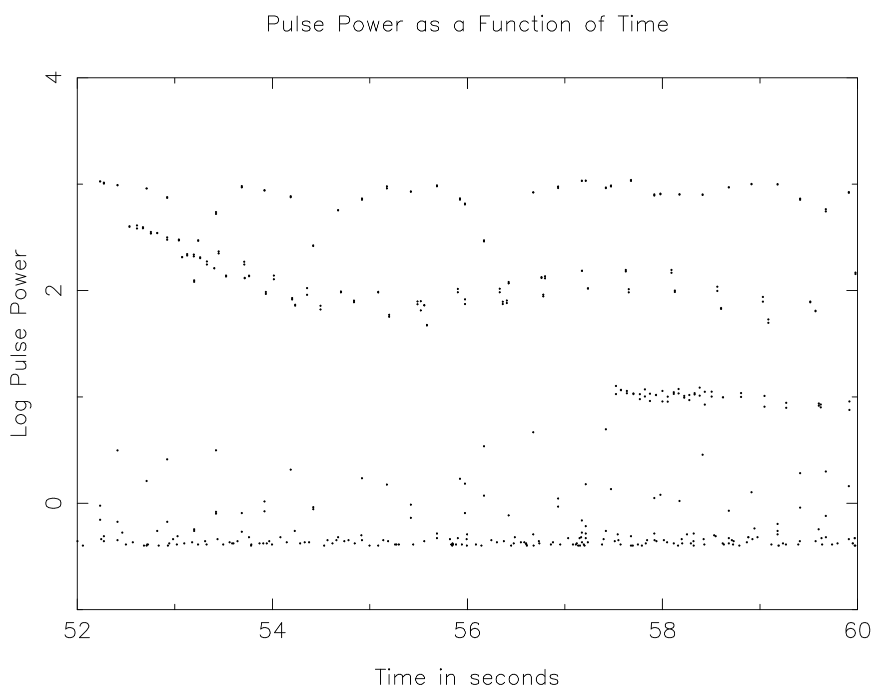

Figure 7: Pulse intensity vs time at 1144 MHz (DME Channel 121) recorded on January 27, 2004 with the GBT L-band receiver. Individual pulses in each pulse pair are shown.

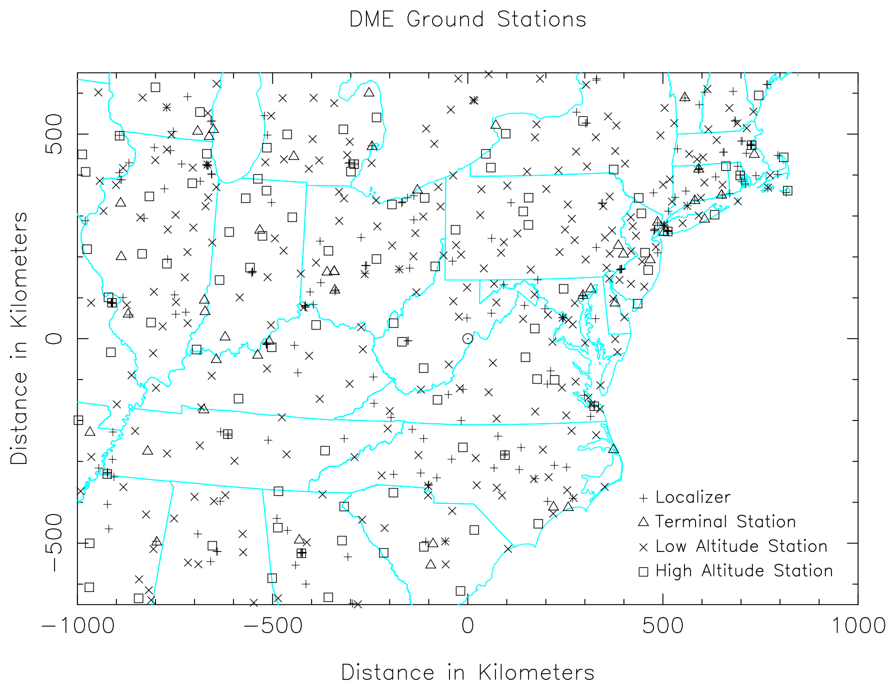

Figure 8: The locations of all DME stations found in the Digital Aeronautical Information CD data base. The high altitude stations are marked with squares, the low altitude stations are marked with X's, the terminal stations are marked with triangles, and localizer stations are marked with +'s.

in the 0.25 MHz bandwidth of the pulse. In Section 2 we calculated this threshold to be -151.6 dBW at the GBT receiver input with a noise temperature of 20 Kelvins. The stated receiver sensitivity of a commercial DME ground station is -117 dBW [5]. If we assume that the system noise temperature of the DME station is 400 K, then the GBT detection threshold used is about 21.6 dB $= 151.6 - 117 - 10 * Log_{10}(400/20)$ lower in terms of system noise power than is used in the DME station receiver. The DME ground station detection threshold would correspond to a level of about 1.8 on the vertical scale of Figure 7. One might guess that this threshold difference is roughly the signal processing margin used in the DME station receiver to avoid false detections or detections of distant aircraft interrogating other stations on the same frequency.

4 Ground Station Locations

Figure 8 shows the location of all DME stations in the eastern U. S. around Green Bank that are found in the Navaid Digital Data File of the Digital Aeronautical Information CD data base from the National Aeronautical Charting Office of the Federal Aviation Administration [9]. Stations with different service radii and altitude ranges are shown with different symbols.

An example of the locations of only stations on the same DME channel is shown in Figure 9. The large circles illustrate the greater range of the high-altitude stations. Around the location of Green Bank two irregular contours show the line-of-sight distance to an aircraft just above the horizon as seen from the prime focal point of the GBT for aircraft altitudes of 15,000 and 35,000 feet above sea level. The horizon contours do not take atmospheric refraction into account, but refraction extends the effective line-of-sight range by only 5 to 10%. For a full set of single channel DME location maps see the web site

http://www.gb.nrao.edu/ rfisher/DME/dme_sta_map.html

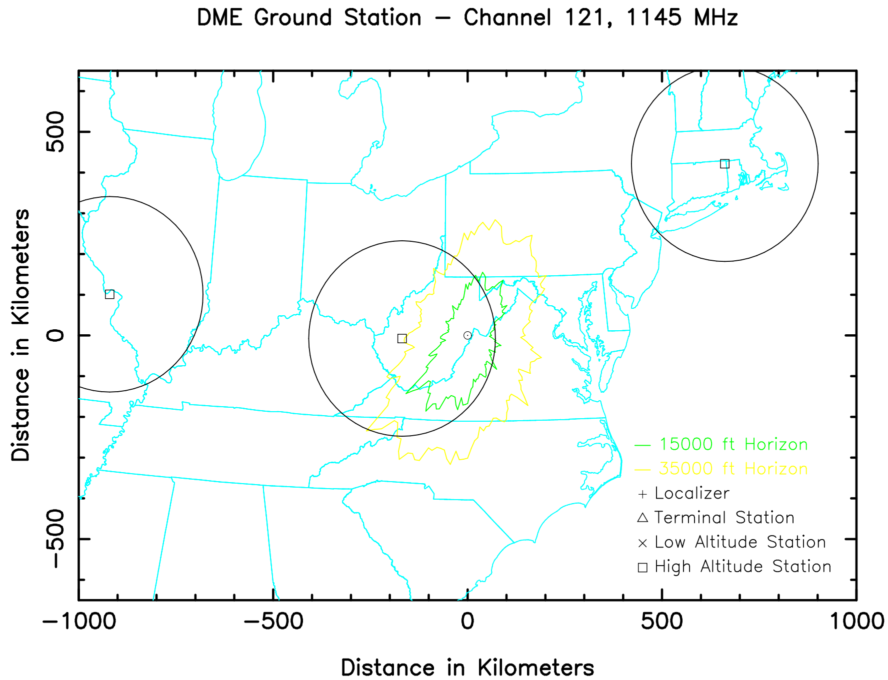

Figure 9: The locations of DME channel 121 (1144 MHz) stations. The high altitude stations show 240 km range circles. The low altitude station show 74 km radius circles, the terminal stations are enclosed in 46 km radius circles, and the localizer stations are drawn with 20 km radius circles. The irregular contours around Green Bank show the line-of-sight horizons of the GBT prime focus point for two different aircraft altitudes.

5 Pulse Detection and Statistics

To generate a test data set under conditions close to typical GBT observing I ran a series of on-off scans on the radio source 0952+176 which has a continuum flux density of about 1.4 Janskys and a narrow HI absorption line at 1147.5 MHz with a depth of about 15 mJy [14]. These observations used 8-bit baseband sampling of a 10 MHz bandwidth centered on 1147 MHz. This passband included DME channels 119 (1141 MHz) through 126 (1150 MHz) plus channel 118 at the lower edge of the band and a bit of spectrum above the air-to-ground frequency range. Each on-source and off-source scan was 5 minutes long, and there were 12 on-off pairs from which a total on or off integration time of 54 minutes was obtained. A few data records were spoiled by sampling glitches and a blast of wideband interference that lasted a couple of minutes. The observing session ran from about 05:24 to 07:37 EST (13:29 to 15:42 LST).

These data were processed in one-minute chunks, which was the file size into which the data acquisition computer divided the 8-bit samples. The A/D input level was such that the noise voltage rms value spanned about four A/D levels. The sample interval was 50 nanoseconds (20 MS/s). The spectrum looked roughly like the one in Figure 3 except with a center frequency of 1147 MHz.

The first major signal processing step was to scan every one-minute data file for pulses and create a list of pulse times and intensities for each DME channel in the spectrum. The pulse detection scheme was similar to the methods described in Zhang *et al* [11] [12] and Singhal [13], which was to Fourier transform one-megasample (50 millisecond) data lengths into the frequency domain, apply a matched filter to each DME frequency, transform back to the time domain, square to get power, and search this power sample series for peaks above a chosen threshold. After some experimenting with false detections on random noise, the chosen threshold was set to 15 times the median power value in the first 50-millisecond sample of each DME channel. This was roughly 10 times the average power level in a channel filter passband between pulses. Pulse peaks were then found starting with the strongest one. Data in a 15-microsecond window centered on the found peak were set to zero so that this pulse and surrounding data would not be detected in the remainder of the peak search. This window was small enough to allow the second pulse in a 12-microsecond pair to be detected but wide enough to suppress most of the wings of strong pulses. The final pulse list was sorted by pulse time for further analysis and for use in blanking pulses in the original data set.

During the analysis of pulse statistics the strongest pulses were found to affect the entire 10-MHz spectrum causing false detections in channels other than the one containing the transmitted pulse. To remove this spurious effect from the analysis the sorted pulse lists were searched for strong pulses, and all pulses in other channels within five microseconds of each strong pulse were deleted from the list.

The filter applied to each DME channel frequency was chosen by visually matching the envelope of the spectrum shown in Figure 5 to a gaussian function. This function had a full-width-half-maximum width of 0.25 MHz in the voltage domain. This corresponds to a power noise equivalent width of 0.188 MHz. If a DME pulse transmitter were as much a 0.1 MHz off in frequency, as is permitted in at least one manufacturer's specs, the filter response would be down by about 4 dB, but most of the pulses appear to be within about 30 kHz of the nominal channel frequencies.

We expect pulses to arrive in pairs, either 12 or 36 microseconds apart for mode X or Y, respectively. This should be evident in a histogram of adjacent pulse separations. Figure 10 shows four such histograms for one minute of measurements of four different DME channels. All four channels show a clear peak at 12 microseconds, and channel 126 shows a small number of mode Y pulses at 36 microseconds. The nearest ground station assigned to channel 124 is in Beckley, WV so there is a lot of activity on this channel. The large number of pulses at spacings other than 12 microseconds may be due to echoes of strong pulses from terrain around Green Bank as described in Section 7. Several channels in the spectrum survey from 1100 to 1150 MHz showed a background pulse spacing distribution which was essentially independent of spacing. The source of these pulses remains to be investigated.

Figures 11 and 12 show examples of the distribution of the number of pulses detected in one five-minute scan as a function of pulse intensity between the detection threshold and the pulse saturation limit of the GBT receiver for eight DME channels. The solid and dashed lines in these plots show the difference between all detected pulses and only pulses that have detected neighbors near 12 microseconds away. The difference gives an upper limit on the number of false detections due to random noise or sources of non-DME pulses. An interesting feature of these plots is that the number of known pulse pairs per logarithmic intensity interval does not appear to be rising steeply with decreasing intensity near the detection limit. This is fairly typical of most of the data in this two hours of GBT observations.

Two important questions to ask are how much power remains in pulses below the detection threshold, and is this sufficient to see in the spectrum with detected pulses removed? To answer these questions we need to assume a number distribution for the undetected pulses as a function of intensity. Assuming a power law

$$log(\frac{n(I)}{n_o}) = \alpha\ log\left(\frac{I}{I_o}\right) \tag{3}$$

or

$$\frac{n(I)}{n_o} = \left(\frac{I}{I_o}\right)^\alpha \tag{4}$$

then the total power in the undetected pulses will be

$$p = \sum_i n(I_i)\ I_i = \sum_i n_o\ \left(\frac{I_i}{I_o}\right)^\alpha\ I_i \tag{5}$$

If we do the summation using logarithmic intervals in I_i of 0.1 for various values of α we get the values of p/I_o shown in the second column of Table 1. For example, for $\alpha = 0$, if I_o is the pulse power detection threshold and $n_o = 1$, the cumulative power from all pulses below the threshold will be 4.9 times the power in one pulse at the threshold level. For values of $\alpha \leq -1$ the summation in Equation 5 will diverge at low intensities, and such a distribution will give infinite power without a low intensity cutoff. Since each DME channel will be occupied by a finite number of aircraft such a divergence is not possible in practice.

To determine limits on the number of pulses under the detection threshold that can be tolerated in an astronomical spectrum let's assume a five-minute integration with a spectral resolution of 20 kHz (5.2 km/s at 1.15 MHz). The rms noise power in each spectral channel will be 4.1×10^{-4} times the total noise power in the channel. From experiments with the GBT data we know that most pulses can be detected at a level of 15 times the average noise power in the bandwidth of the pulse. The width of one pulse is 3.5 microseconds

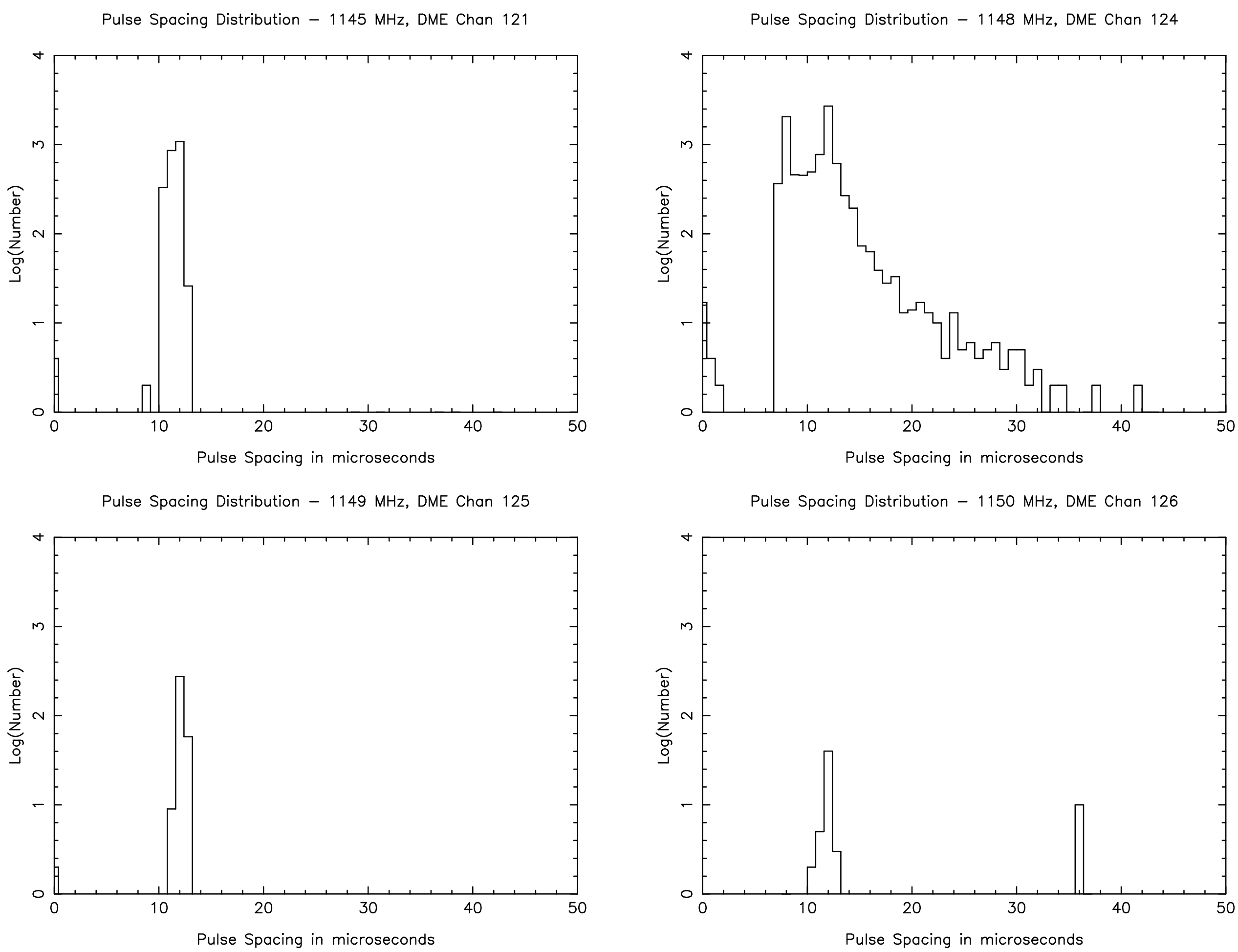

Figure 10: Distribution of adjacent pulse spacings for four DME channels measured for one minute near 06:22 EST on January 27, 2004.

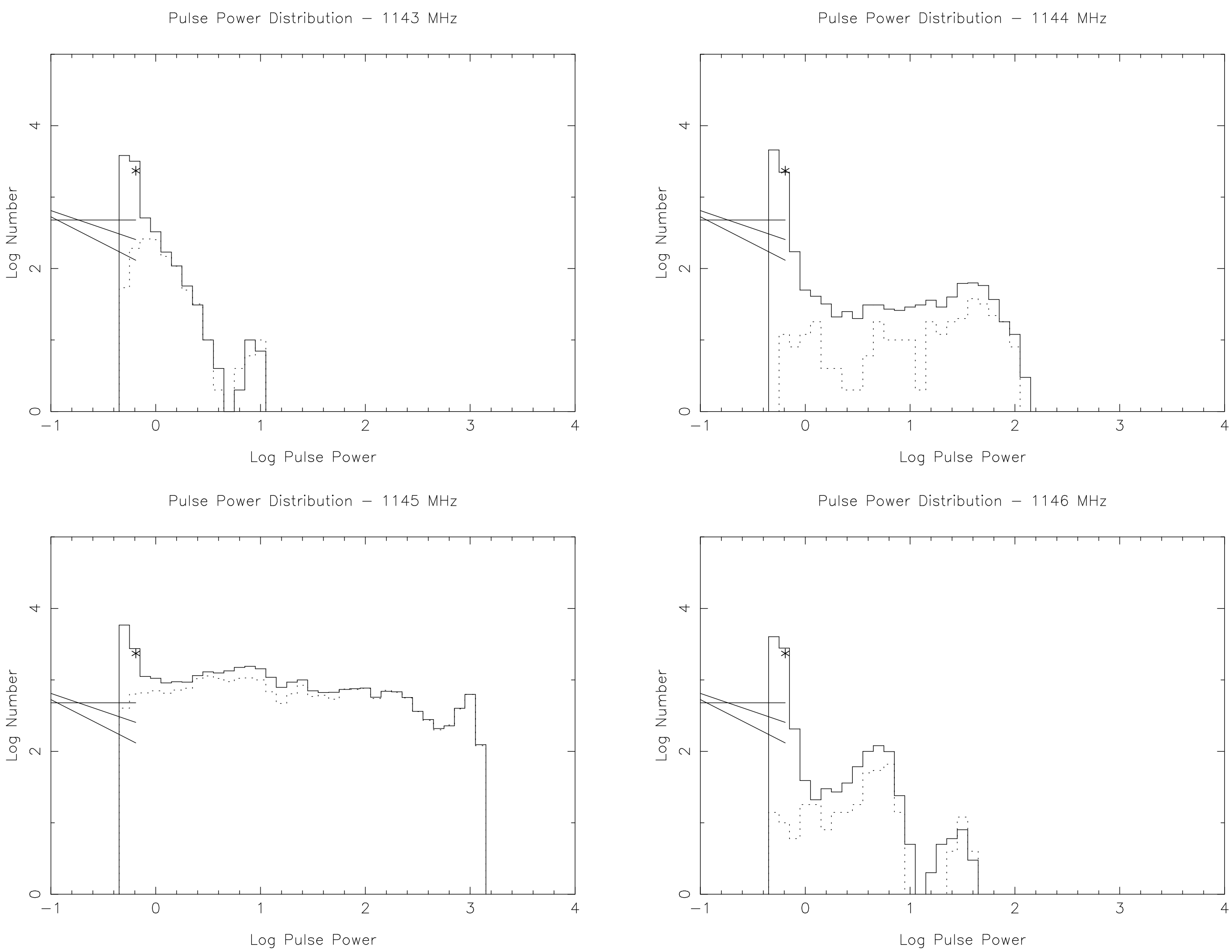

Figure 11: Number distribution of detected pulses as a function of pulse intensity for DME channels 119-122 in a five minute scan recorded at 06:22 EST. The solid lines show all detected pulses, and the dashed lines show only pulses that are paired with another between 11 and 13 microseconds away. On the left side of each plot are plotted the pulse number distribution limits to remain undetected in a five-minute integration as described in the text. The star marks the limit if all unblanked pulses are at the detection threshold. The horizontal straight line is for a number density index of $\alpha = 0$, and the sloped lines are for $\alpha = -0.5$ and -0.75.

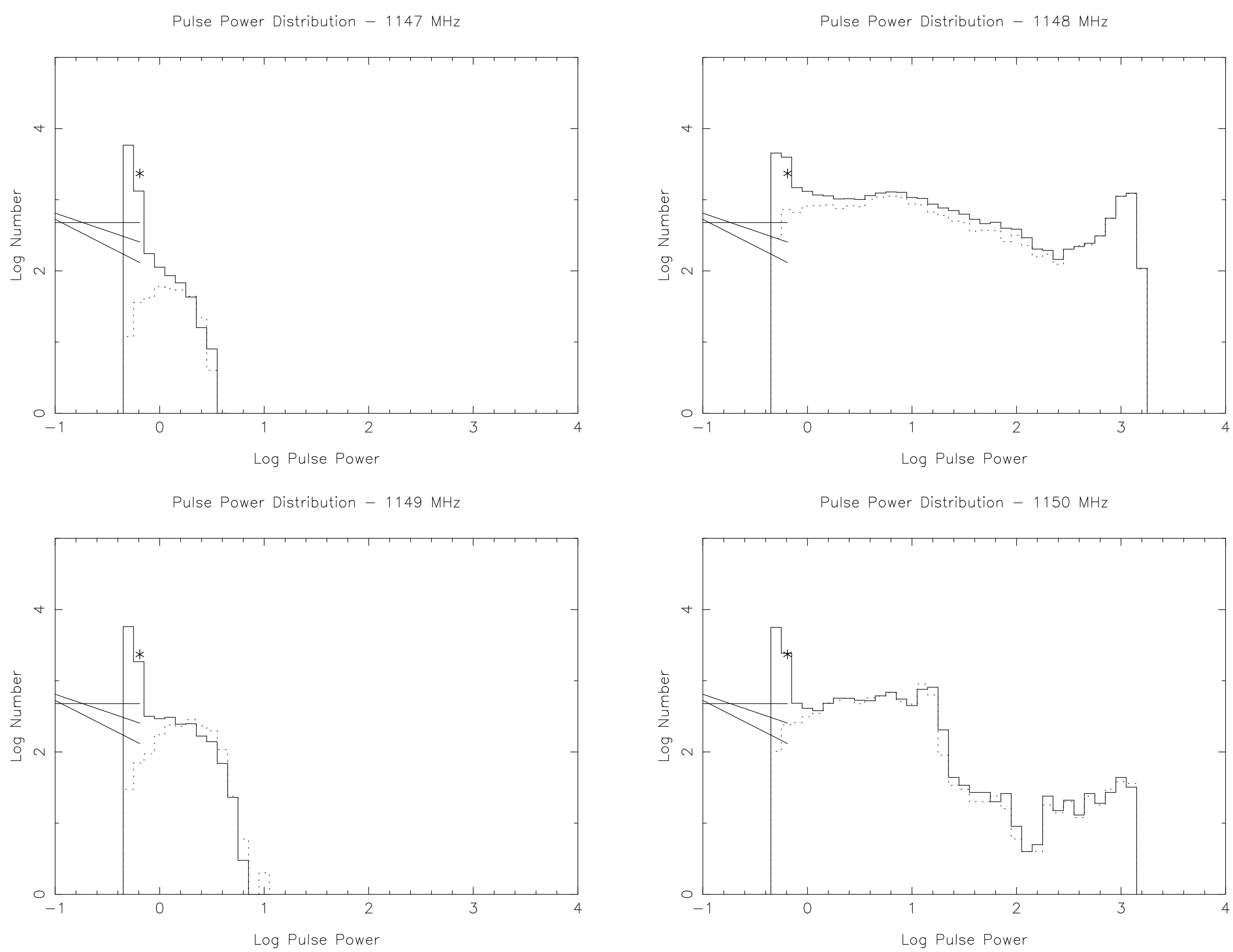

Figure 12: Same as Figure 11 except for DME channels 123-126.

Table 1: Undetected pulse residual power and limits on the number of pulses per second in the interval just below the detection threshold in a 300-second integration for different pulse intensity distributions

α	p/I_o	$N(I_o)/second$
+inf	1.0	7.8
0	4.9	1.6
-0.25	6.3	1.2
-0.50	9.2	0.85
-0.75	17.9	0.43

so the power in one pulse averaged over the 300 second integration is $15 \times 3.5 \times 10^{-6}/300 = 1.75 \times 10^{-7}$ times the noise power in the pulse bandwidth. Hence, there could be $4.1 \times 10^{-4}/1.75 \times 10^{-7} = 2343$ pulses at the detection threshold (7.8 per second) without significantly affecting the spectrum. If the undetected pulse intensities were distributed with a power law of $\alpha = -0.5$, then there could be $2343/9.2 = 255$ pulses (0.85 per second) in the first interval below the detection thresholds and more at weaker intensities according to the power law. The tolerable pulses per second in the interval just below the detection threshold for various values of α are given in the third column of Table 1, and the total pulse number limits are plotted in Figures 11 and 12.

The limits shown on the left side of the plots in Figures 11 and 12 show that the unblanked pulses are close to being detectable in the astronomical spectra for the more active DME channels measured. The assumptions that went into the calculation of these limits may be a bit pessimistic. In an on-off observing procedure the average pulse power will tend to cancel, and the one-sigma intensity limit is probably a bit too stringent. Nevertheless, the unblanked pulses are of some concern, and improvements in pulse detection sensitivity may be worth pursuing. For a given pulse intensity distribution, the number of tolerable pulses below the detection threshold is inversely proportional to the threshold intensity.

6 Signal Intensity vs DME Station Distance

One might expect to measure lower average signal intensities on DME channels where the nearest ground station is farther away. To test this assumption I plotted the relative average intensity, summing all pulses, as a function of nearest station distance. The results are shown in Figures 13 and 14 for all channels shown in Figure 2 above 1100 MHz in the five minutes on each spectrum segment.

A notable feature of Figure 13 is that relatively strong signals can be seen for stations out to 500 kilometers distance, particularly for high-altitude stations. There may be saturation effect in the intensity of signals from nearby stations so the upper envelope of the distribution may be somewhat suppressed at short distances. As expected, the signals associated with low-altitude stations are generally weaker than those associated with high-altitude stations. Keep in mind that all signals are not coming from aircraft that are interrogating the nearest station so we can draw conclusions only from trends in these figures and not from individual data points. For example, the intensity assigned to the terminal station at a distance of about 470 km might be due to signals from aircraft that are interrogating more distant stations.

In ten of the measured DME channels signals were detected from mode Y transmissions as inferred from prominent groups of pulse spacings near 36 microseconds. Since this mode is infrequently used, these points are given a different symbol in Figures 13 and 14. Five of these channels did not have mode Y stations listed in the NACO data base. Either the data base is incomplete, or we are left to puzzle about the origin of these signals.

The see how the DME signal power in each channel varies over a couple of hours the total power of all pulses that have pairs at 12 microseconds spacing in one-minute intervals are plotted in Figures 15 and 16. These data are from the January 27, 2004 GBT run on quasar 0952+176. The channels with the greatest DME pulse power tend have a more constant power than the ones with less power. This is likely due to the fact that the channels with less DME power have fewer aircraft contributing pulses, and occasionally no aircraft are visible in these channels. There is a general tendency for the total pulse power to increase with

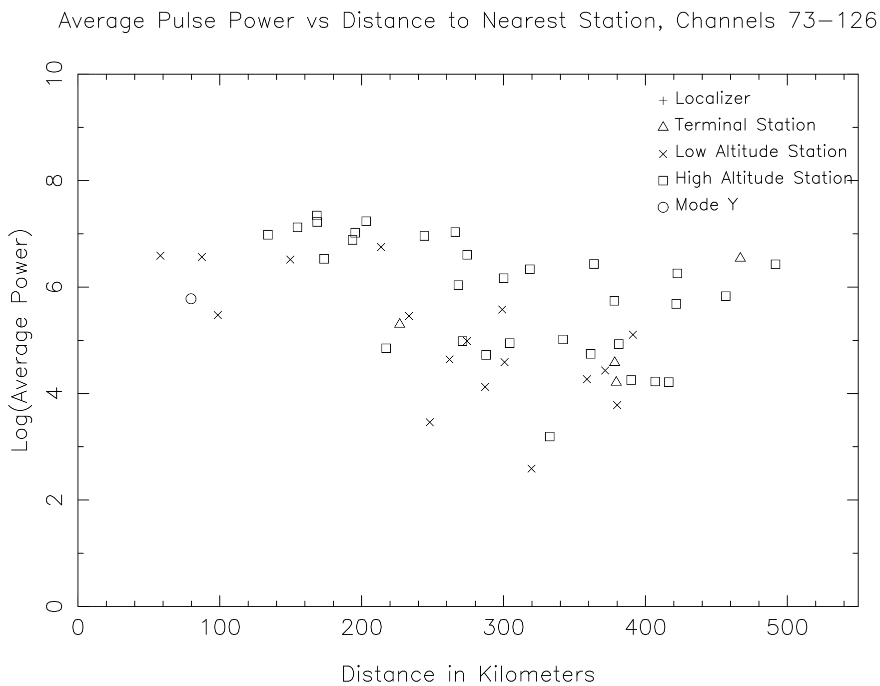

Figure 13: Relative average signal power in five minutes as a function of the distance to the nearest DME station from Green Bank for all DME channels above 1100 MHz shown in Figure 2. The high, low, terminal and localizer station symbols are the same as in Figures 8 and 9.

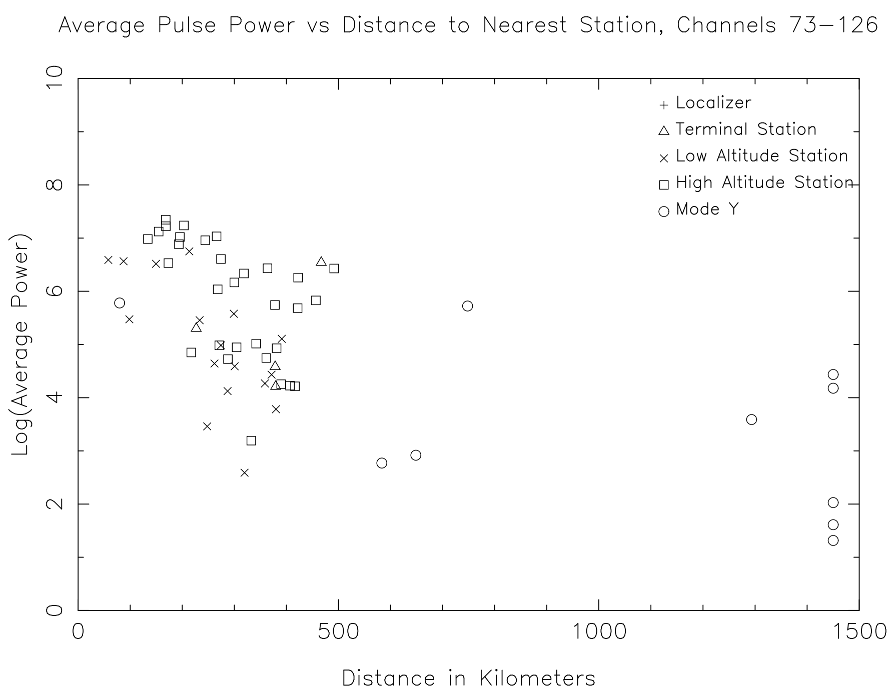

Figure 14: Same as Figure 13 except for a longer distance range. There are very few mode Y stations and few mode Y signals detected so these are given a separate symbol. No stations were listed in the NACO database for five of the mode Y channels in which signals were detected. These are plotted on the right side of the figure.

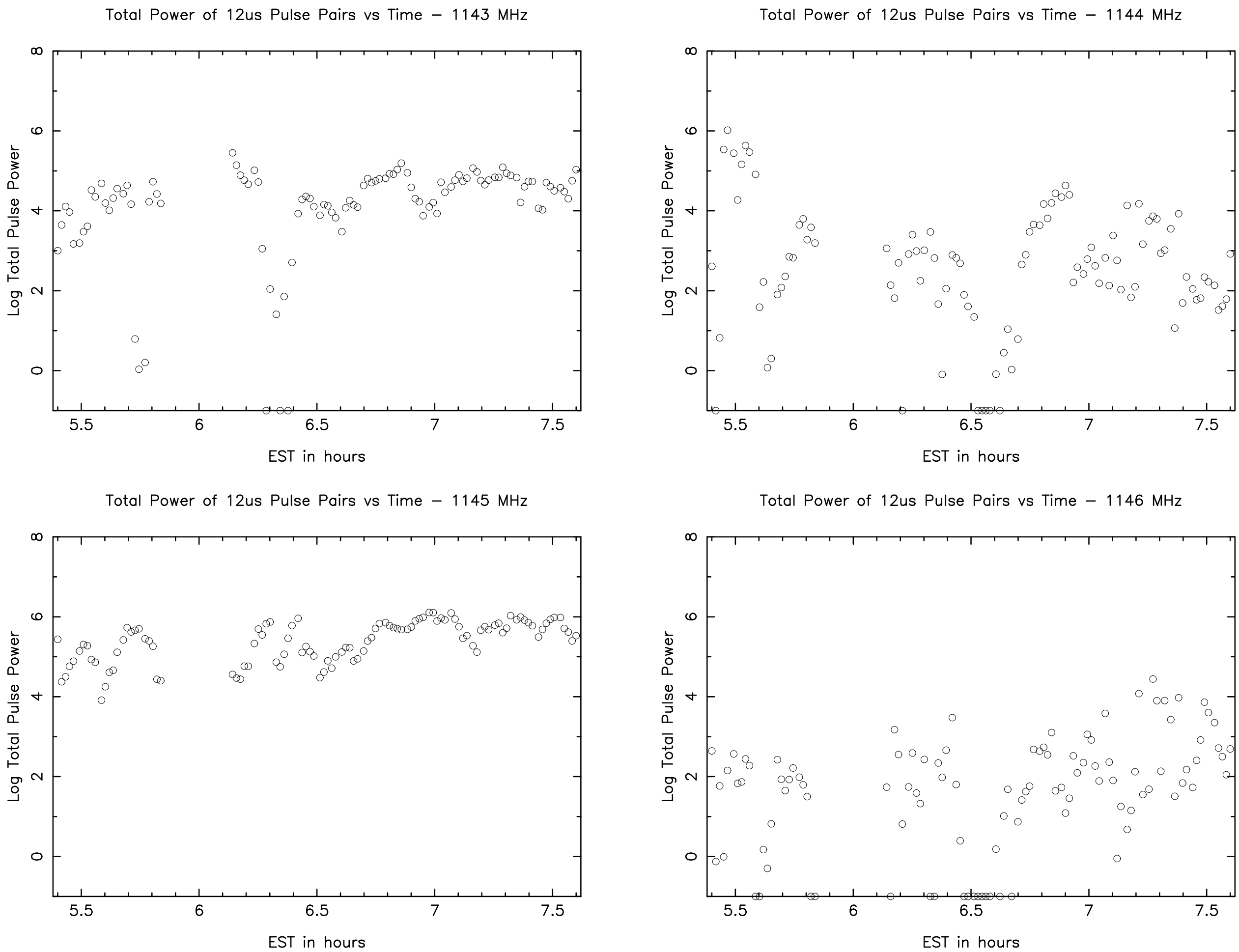

Figure 15: Total DME pulse power with 12 microsecond pulse spacing in one-minute intervals for DME channels 119-122 as recorded on January 27, 2004 on the GBT.

time as one might expect in the early morning hours as more aircraft begin their flight schedules.

7 Echoes

The broad distribution of pulse spacings shown in the top right panel of Figure 10 could be due to echoes of strong pulses from surrounding terrain as were measured in pulses from a ground-based air surveillance radar [10]. To test this hypothesis average pulse power profiles were computed in a number of one-minute intervals for the strongest pulses that did not saturate the receiver system. The results for the two DME channels with the largest number of strong pulses are shown in Figures 17 and 18. Figure 18 is for the same DME channel as the top right panel of Figure 10. All of the profiles show strong evidence of echoes out to a delay of about 70 microseconds. This agrees well with the distribution of radar pulse delays shown in Figure 11 of [10]. Echo pulse intensities relative to the direct pulses range from about -20 dB at small delays to less than -40 dB, which is the detection limit of these measurements. The red trace in Figure 18 shows what could be an isolated single reflection at a delay of about 45 microseconds.

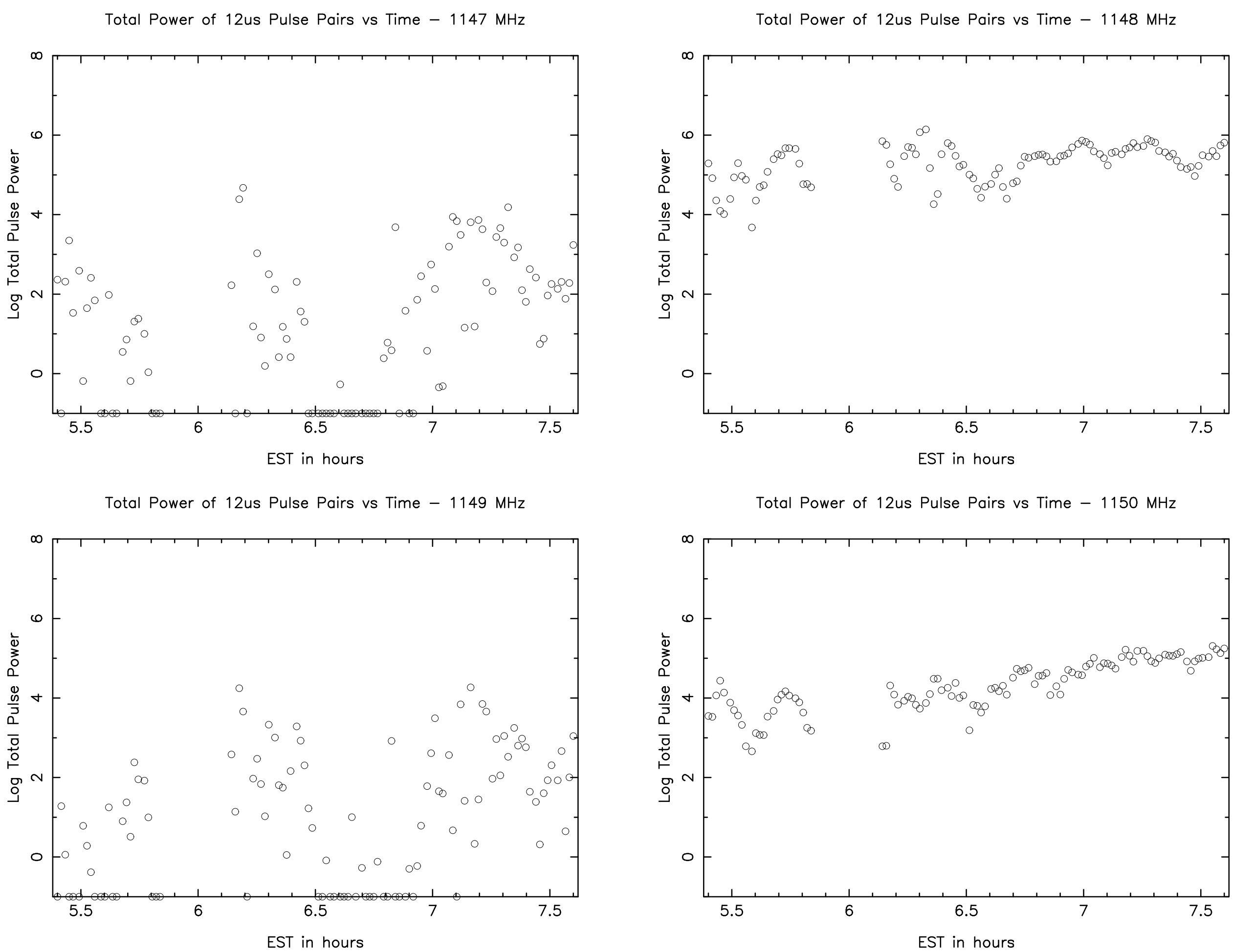

Figure 16: Total DME pulse power with 12 microsecond pulse spacing in one-minute intervals for DME channels 123-126 as recorded on January 27, 2004 on the GBT.

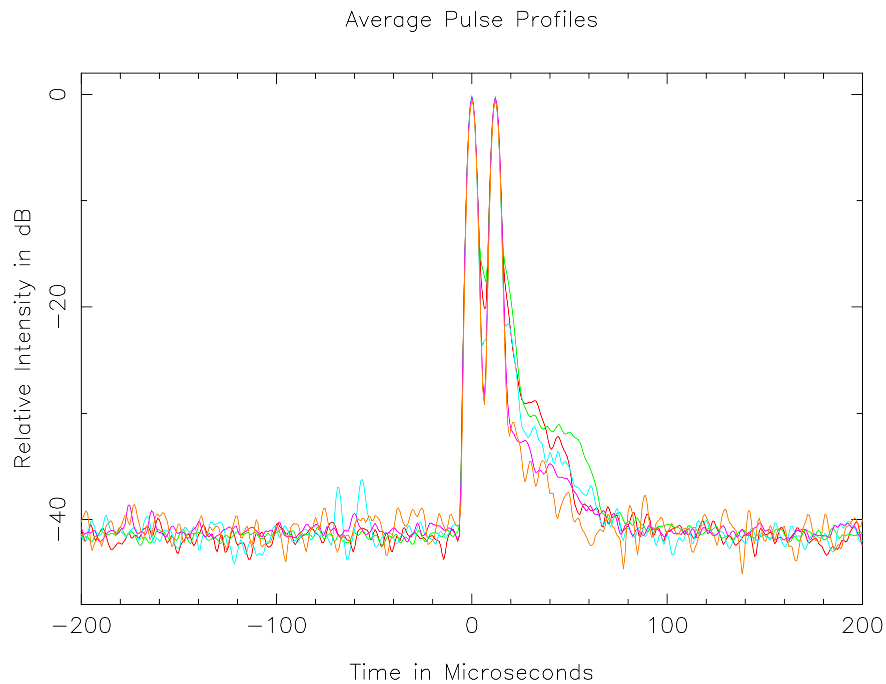

Figure 17: Average pulse profiles at 1148 MHz (DME channel 124) in one minute scans recorded at 05:24 (red), 06:11 (green), 06:33 (blue-green), 07:06 (violet), and 07:27 (orange) EST of January 27, 2004. Only isolated pulses in a 2-dB range of amplitudes just below GBT receiver saturation were included in the averages.

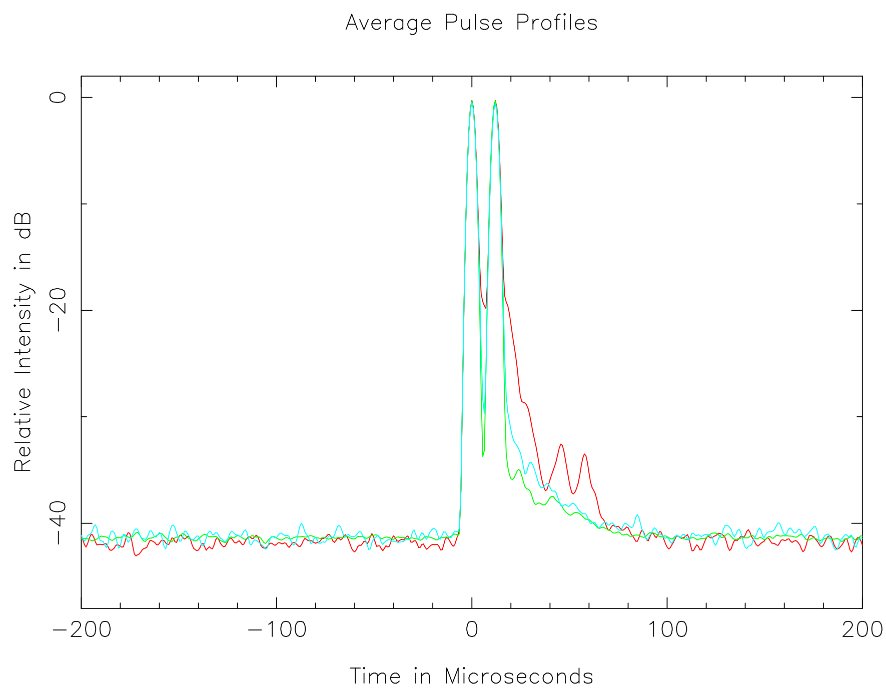

Figure 18: Average pulse profiles at 1145 MHz (DME channel 121) in one minute scans recorded at 05:24 (red), 07:06 (green), and 07:27 (blue-green) EST of January 27, 2004. Only isolated pulses in a 2-dB range of amplitudes just below GBT receiver saturation were included in the averages.

8 Pulse Blanking in the Integrated Spectra

To remove DME signals from the data the list of detected pulse times in each one minute record were used to set blanking windows in the raw sampled data. Each blanking window was 12 microseconds wide, and it was applied to each detected pulse, including a small fraction of false detections due to random noise. This is similar to the blanking method described in Zhang *et al* [11]. A detected pulse in any of eight DME channels (1143-1150 MHz) resulting in blanking data for the full 10 MHz bandwidth. In the January 27 data this resulted in a blanked data fraction ranging from 0.5 to 1.1% of the data samples with the fraction increasing with time over the 05:24 to 07:37 EST observing period. A smaller fraction of data could be blanked if one-megahertz sections were processed separately, blanking only on pulses pulses from one DME channel at a time. However, this adds the complication of stitching the spectra back together seamlessly, and strong pulses from adjacent channels that splatter across the spectrum may not be blanked as effectively. Even in the busiest part of the day the data lost probably will not be greater than about 2% with full 10-MHz spectrum blanking. Simultaneous processing of wider bandwidths would lose proportionately greater fractions of data.

One consequence of blanking small windows of sampled data is that power is lost, and extra sidelobes will be generated on narrowband signals. The fraction of power lost and the total power in the sidelobes will be equal to the blanking fraction. One or two percent usually will not affect the astronomical data significantly, but this effect needs to be kept in mind. In principle, one can compute and correct for the sidelobe pattern and power loss from the known blanking pattern, if the extra computational load is warranted.

Figure 19 shows the total power spectrum of one minute of data. Strong DME signals can be seen in the top spectrum, without blanking, in four of the channels, and weak signals can be seen in at least three others, not including the channel at 1142 MHz. The middle trace shows the spectrum from the same data with pulse blanking. To the noise level of this spectrum, all of the blanked DME signals have been suppressed. There are still a few RFI signals in the spectrum, but most of them are quite narrow and can be excised by deleting one to three spectral channels around each narrow spike as shown in the bottom spectrum. None of the narrow spikes are likely to be associated with the DME signals.

To test how well pulse blanking works on long astronomical integrations the data from two, two-hour observing sessions of the quasar 0952+176 were run through the blanking algorithms. The sessions were on January 27, 2004 from 05:24 to 07:38 EST (13:29-15:43 LST) and February 23, 2004 from 17:32 to 20:01 EST (03:25-05:54 LST). This radio source has a continuum flux density of about 1.4 Janskys and a narrow HI absorption line at 1147.5 MHz with a depth of about 15 mJy. The observing sequence was alternately 5 minutes on source and 5 minutes off. The total on- plus off-source integration times in the sessions were 108 and 140 minutes, respectively. The data were summed with weighting of each spectrum by the inverse of the square of the estimated system temperature for each ten-minute on-off scan pair. The weighted system temperature estimates in each session were 21.8 and 23.4 Kelvins, respectively. The second session was observed at lower elevation angles.

Figures 20 and 21 show the integrated spectra from the two observing sessions with and without pulse blanking and narrowband spike removal. The vertical scale is in fraction of the system noise power. The weak absorption feature at 1147.5 MHz can be seen in the blanked spectra. There is a hint of residual DME signal in the strongest channel frequencies as we expect from the analysis in Section 5, but this doesn't affect the detection of relatively narrow spectral features very much.

Figures 22 and23 show the differential Doppler shift in the HI line frequency between the two observing sessions. The combined spectrum in these figures has had the February 23 spectrum shifted by the expected 52 kHz before taking the weighted average of the two spectra. The vertical scale in Figure 23 is shown approximately in Janskys. The continuum level around 0.95 Jy is less than the published 1.4 Jy, but the measured peak line depth to continuum ratio is quite close to the published value of 0.013 by Kanekar and Chengalur [14].

9 Computational Requirements and Future Work

All of the signal processing described in this report was done on a Xeon general purpose processor with a clock speed of approximately 2 GHz. The computationally intensive code was written in C/C++, and the main

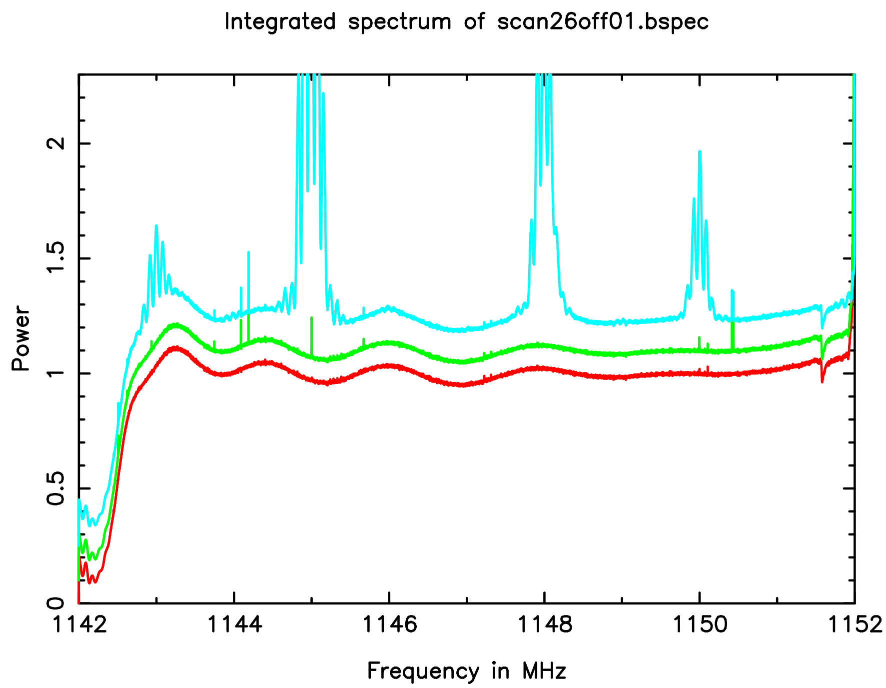

Figure 19: Total power spectra computed for one minute of data recorded at 07:23 EST on January 27, 2004 on the GBT. The spectra contain 8192 channels (1.2 kHz channel spacing). The top (blue-green) trace is without blanking. The middle (green) trace is with blanking, and the bottom (red) trace is with blanking and narrowband signal removal.

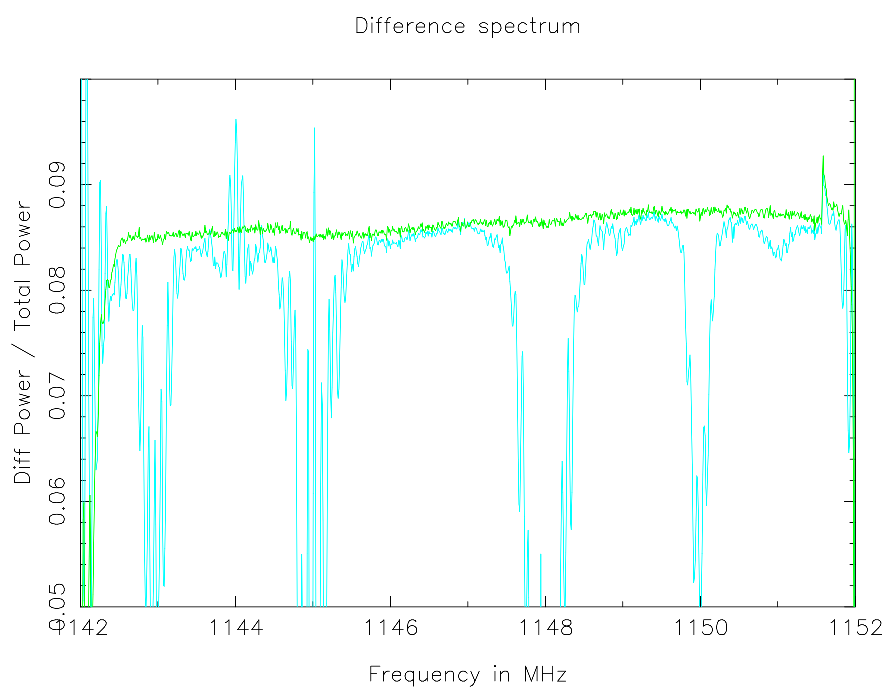

Figure 20: Averaged (ON - OFF) / OFF spectra for all of the January 27 data. The bottom (blue-green) spectrum is without blanking and the top (green) spectrum is with blanking and narrowband spike removal.

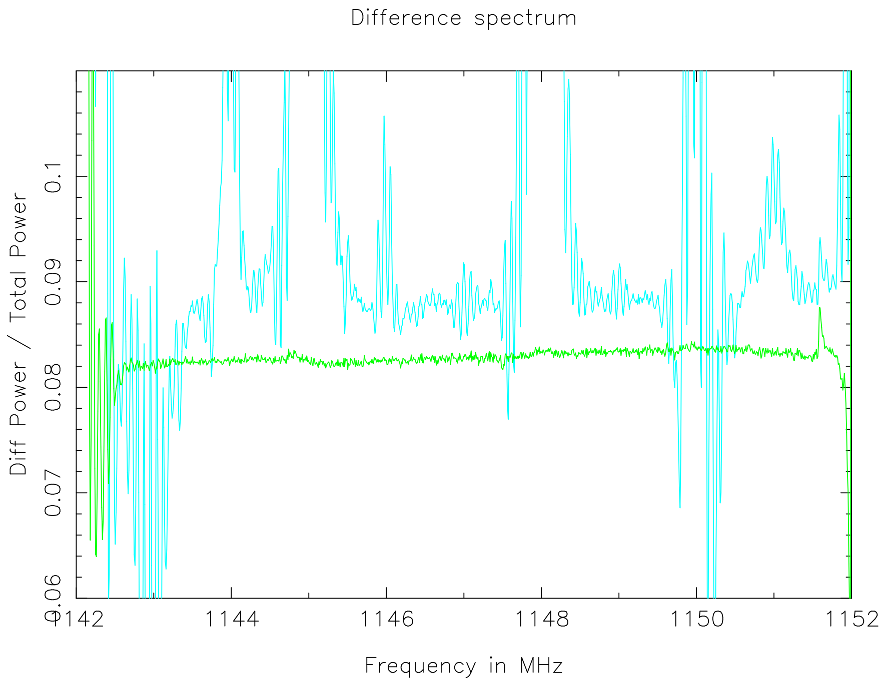

Figure 21: Averaged (ON - OFF) / OFF spectra for all of the February 23 data. The bottom (blue-green) spectrum is without blanking and the top (green) spectrum is with blanking and narrowband spike removal.

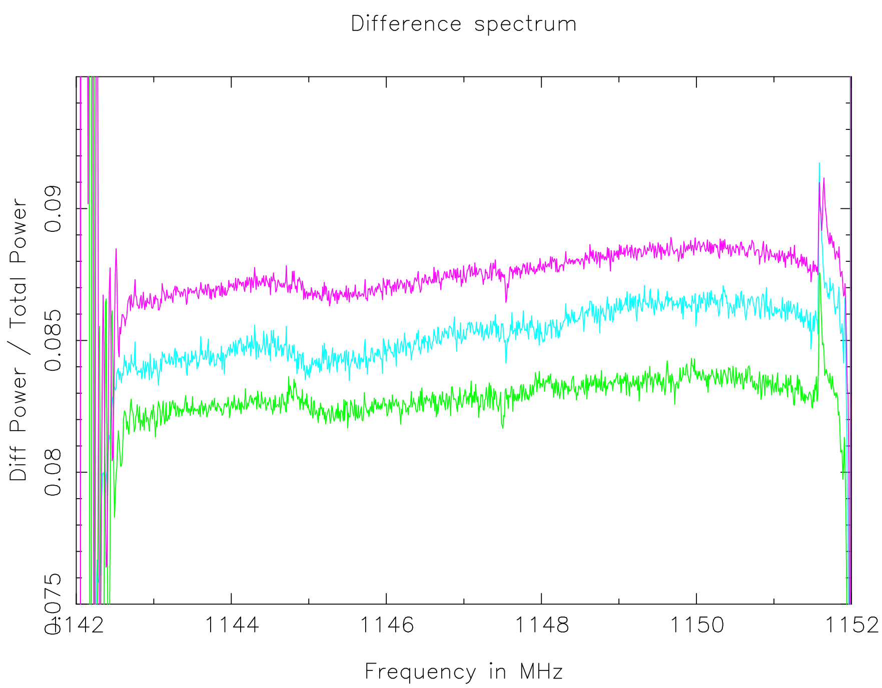

Figure 22: Averaged (ON - OFF) / OFF spectra for all of the data with blanking and narrowband spike removal. The bottom (green) spectrum is from January 27 middle (blue-green) spectrum is from February 23, and the top (violet) spectrum is the average of all data with the February 27 spectrum shifted by the expected differential Doppler shift. The spectra are offset vertically by a small amount for clarity.

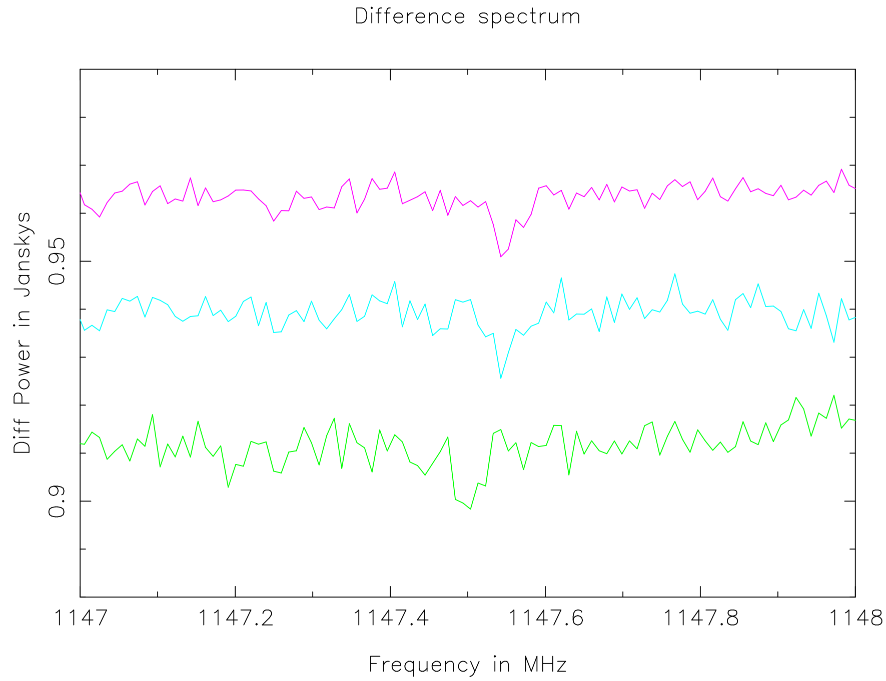

Figure 23: Same as Figure 22 but expanded around the 1147.5 MHz HI absorption feature and with the vertical scale in Janskys. The spectra are offset vertically by a small amount for clarity.

FFT code was reasonably well optimized to avoid inefficiencies such as redundant coefficient calculations. With this processing environment finding DME pulses in the data required about 52 minutes of CPU time for one minute of 20 MS/s data. Computing integrated power spectra with pulse blanking and a 25% overlap in FFT input data required about 8.5 minutes of CPU time for each minute of data. The pulse-finding computation time might be reduced by a factor of two or three with better algorithms, but this will still be a factor of 30 or so slower than real time, and it will scale linearly with processed bandwidth. Hence, a routinely useful system for observing in the presence of DME interference will require dedicated hardware, such as one or more of the largest FPGA chips.

More sensitive pulse detection will help remove weaker pulses that are probably leaking into the pulse-blanked spectra shown in this report. The filter used to optimize pulse detection is reasonably close to optimum so the only route for weaker pulse detection is an antenna and RF amplifier system that has a higher signal-to-noise ration on DME signals. If we assume that the GBT has a sidelobe gain of -15 dBi and a system temperature of 20 Kelvins, then one can realize about 8 dB increase in SNR with a +6 dBi antenna gain and a system temperature of 400 Kelvins. Plans to try such a receiving system for this purpose are now underway.

References

[1] Forssell, B., 1991, Radionavigation Systems, Prentice Hall, New York

[2] Kline, P. A., 1997, Atomic Clock Augmentation for Receivers Using the Global Positioning System, PhD Thesis, Virginia Polytechnic Institute and State University, http://scholar.lib.vt.edu/theses/available/etd-112516142975720/unrestricted

[3] Van Vliet, L. J., Rieger, B., Verbeek, P. W., Fourier Transform of a Gaussian, www.ph.tn.tudelft.nlx/ lucas/education/tn254/2002/ Fourier

[4] http://www.census.gov/geo/www/cob/st2000.html

[5] http://www.amsjv.com/publications/ASI11181119SLqx.pdf

[6] http://www.rockwellcollins.com/ecat/br/DME-42_442.html?smenu=103

[7] http://www.rockwellcollins.com/ecat/br/DME-4000.html?smenu=103

[8] http://www.flightsimaviation.com/index.php?p=aviationtheory&ch=6

[9] http://www.naco.faa.gov/index.asp?xml=naco/catalog/charts/digital/daicd

[10] http://www.gb.nrao.edu/ rfisher/Radar/analysis.html

[11] Zhang, Q., Zheng, Y., Wilson, S. G., Fisher, J. R., Bradley, R. F., 2003, Combating Pulsed Radar Interference in Radio Astronomy, Astron. J., vol. 126, pp. 1588-1594

[12] Zhang, Q., Zheng, Y., Wilson, S. G., Fisher, J. R., Bradley, R. F., 2004, Removal of DME Interference from Radio Astronomy Data, in preparation

[13] Singhal, A., 2004, Detection of AAtomic Hydrogen in Distant Galaxies in the Presence of Radar Interference, University of Virginia Astronomy Dept. Masters Degree project report, June 18, 2003.

[14] Kanekar, N. and Chengalur, J. N., 2001, HI 21 cm absorption in low z damped Lyman-α systems, astro-ph/0101402 v1, 23 Jan 2001.